
Analysis of the ICE Model

Anupam Prasad Vedurmudi



München 2013

Analysis of the ICE Model

Anupam Prasad Vedurmudi

Dissertation
an der Fakultät für Physik
der Ludwig-Maximilians-Universität
München

vorgelegt von
Anupam Prasad Vedurmudi
aus Kolkata, Indien

München, den June 11, 2013

Erstgutachter: Prof. Dr. J. Leo van Hemmen

Zweitgutachter: Zweitgutachter

Tag der mündlichen Prüfung: Prüfungsdatum

Contents

Abstract	xi
1 Introduction	1
2 The ICE Model	3
2.1 Description of the Model	4
2.1.1 Mouth Cavity	4
2.1.2 Middle Ear System	5
2.1.3 Head Model and External Sound Input	8
2.2 Derivation of the Model	10
2.2.1 Internal Cavity	12
2.2.2 Vibration of the Membrane	15
2.2.3 Vibration of Coupled Membranes	19
2.2.4 Circuit Model	24
3 Evaluation of the ICE–Model	27
3.1 Spatial Vibration Pattern of the Membrane	28
3.2 Cavity Pressure Distribution	30
3.3 Directional Hearing Cues	30
3.3.1 Transmission Gain	30
3.3.2 Internal Time Difference	30
3.3.3 Internal Level Difference	30
4 Conclusion	31
Acknowledgements	35

List of Figures

2.1	Illustration of a gecko's head	3
2.2	Previous and current ICE model representations	6
2.3	Extracolumella Flection	7
2.4	Tympanic membrane model	8
2.5	Previous acoustic head model for geckos	9
2.6	New acoustic head model for geckos	10
2.7	Circular membrane eigenmodes	17
2.8	Sectoral membrane eigenmodes	20
2.9	Low frequency circuit analog	25
3.1	Tokay gecko tympanum vibration profiles.	29

List of Tables

2.1	Functions and Parameters used in the ICE Model	11
2.2	Functions and Parameters used in the ICE Model contd.	12
3.1	Geometry Parameters for the common house gecko (<i>Hemidactylus frenatus</i>) estimated from [5] and the Tokay gecko obtained from [4] and [6].	28

Abstract

Hier steht eine maximal einseitige Zusammenfassung der Dissertation.

Dies ist ein neuer Absatz.

Chapter 1

Introduction

Chapter 2

The ICE Model

Several terrestrial vertebrates, e.g. lizards, frogs, alligators and many birds, possess a hearing mechanism very different to that of mammals: their tympanic membranes are coupled through large eustachian tubes and a large mouth cavity resulting in the influence of the vibrations of one tympanic membrane on those of the other. This is illustrated in 2.1. The typically small head sizes (compared to sound wavelength) of these animals result in small phase differences (ITDs) and negligible amplitude difference (ILDs) between the ears. The coupling serves to enhance the ITDs and create ILDs between the tympanal vibrations. These differences show directionality and serve as hearing cues for localization.

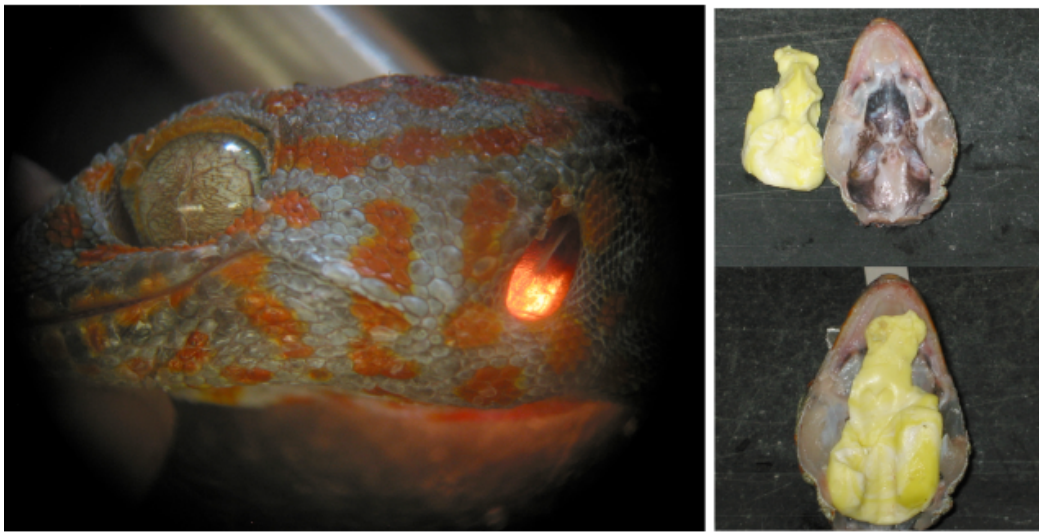


Figure 2.1: Left: Picture of a Tokay gecko's head with the snout pointing to the left. The tympanic membrane is illuminated from behind by a light source on the other side of the head. The cartilaginous extracolumella can be seen attached to the upper part of the membrane. Right: Cast imprint of the mouth cavity of the gecko with the snout pointing to the top. The figures illustrate the coupling of the tympani through the mouth cavity. Photographs courtesy of Jakob Christensen-Dalsgaard.

Proceeding from the earlier work done by Vossen in [1] and [2], in this chapter we present a model for such a system of coupled ears with an emphasis on lizard hearing - specifically the Tokay gecko and the common house gecko. Our goal is to demonstrate its main aspect of such a system - the coupling of the eardrums through the mouth cavity. The main components of such a system are the mouth-cavity, the two tympani and the two *extracolumella* (one on each tympanum). In general, the shape of the mouth-cavity is highly irregular and therefore not conducive to an analytical treatment. Moreover, the system corresponds to a pair of coupled second-order PDE's with moving boundaries. For this reason we will need to make further approximations in order to facilitate an analytic solution.

In order to make the system more analytically tractable we will, as before, study a geometry in which a pair of rigidly clamped linear elastic membranes are coupled through a cylindrical cavity. The cylindrical geometry allows an accurate calculation of the pressure distribution inside the cavity at both low and high frequencies. By accounting for the presence of the asymmetrically attached extracolumella, we will also explain the complex vibration patterns of the membrane. At the end of this chapter, we will have the expressions that describe the steady-state vibrations of both eardrums as a function pressure amplitude, direction and frequency.

2.1 Description of the Model

Before heading to a quantitative analysis of the ICE model, we will first need to list its basic components. and justify their properties based on a realistic mouth cavity.

In Sec. 2.1.1, we will describe the cylindrical model for the mouth cavity and state the reasons for our choice of the geometry and the dimensions used. We will then proceed to describe the middle ear system and its main components of interest, the *extracolumella* and the *tympani* in Sec. 2.1.2. Finally, in Sec. 2.1.3 we will analyse the dependence of the acoustic input to both eardrums on the direction of the sound source, head size and shape.

2.1.1 Mouth Cavity

In the earlier treatment of the ICE model, the mouth canal is modelled as a simple cylinder closed at both ends by rigidly clamped (baffled) circular membranes; these model the tympanic membranes. As shown by Vossen in [1, p. 21] and [2], the length of the cylinder was chosen to be equal to the interaural distance and the radius of the model tympanum is determined from the typical area of the realistic tympanum. The advantage of using a cylindrical cavity model for the mouth cavity is that the pressure distribution inside the cavity is easy to calculate. The pressure distribution inside the cavity becomes highly non-uniform with increasing frequency and a cylindrical cavity simplifies its calculation.

On the other hand, in this description the small area of the tympani results in a cavity volume which is an order of magnitude smaller than that of the realistic mouth-cavity in the corresponding animal. In general, a smaller volume results in a stronger coupling -

both in terms of an increased iTD and an increased iLD. For this reason, the earlier model overestimates the iTDs and iLDs at low and high frequencies respectively.

In order to get around this problem we make some slight modifications to the model. Essentially, we maintain the cylindrical shape of the internal cavity but require it to have a volume which is equal to that of the realistic cavity (V_{cav}). We also maintain the same tympanum size and interaural distance and can therefore calculate the radius of the cylinder as,

$$a_{cyl} = \sqrt{\frac{V_{cav}}{\pi L}} \quad (2.1)$$

where a_{cyl} is the cylinder radius and L is the interaural distance. Simply put, the model consists of a cylindrical shell of radius a_{cyl} and length L with circular holes on either side with the radius of the tympanic membrane, a_{tymp} . These holes are in turn closed by rigidly clamped membranes which will be described in the next section. The previous and current geometric representations of our model are shown in figures 2.2a and 2.2b. The darkly shaded circular surfaces in fig. 2.2b at ends 0 and L correspond to the two eardrums.

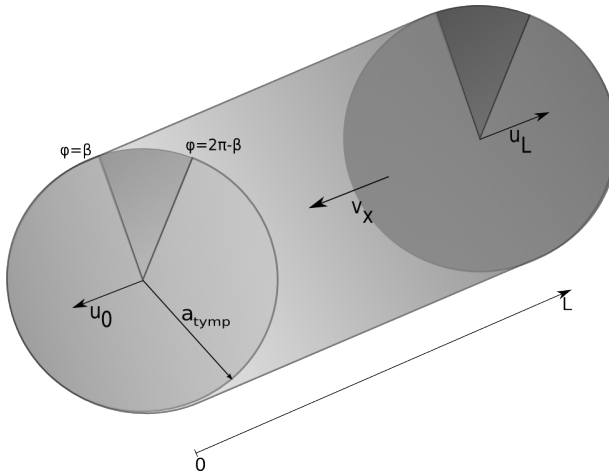
We will be working with the cylindrical polar coordinates, (r, ϕ, x) . The direction along the cylindrical axis is denoted by x and (r, ϕ) are the polar coordinates of the plane perpendicular to the x -direction. Directions outward from the cylinder are taken as positive (in x) and those inward are taken as negative.

2.1.2 Middle Ear System

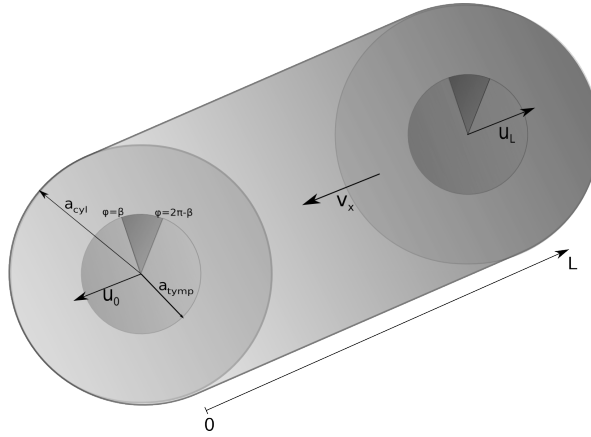
The main components of the middle-ear of lizards are the two eardrums, the columella and the two cartilaginous extracolumella. The tympanic membrane or the eardrum is a thin membrane that separates the outer ear and the middle ear and vibrates in response to external sound waves. Unlike humans, lizards possess only a single middle ear bone, the *columella*, that is connected to both eardrums by means of a cartilaginous element, the *extracolumella*.

The membrane-extracolumella-columella system functions as a second-order lever where the membrane - driven by the internal and external pressures - causes a displacement of the extension of the extracolumella (known as the inferior process). This motion is in turn transmitted via the columella and columellar footplate to the inner ear (cochlea). The inner-ear translates this motion into electrochemical impulses which will be passed on to the brain via the auditory nerve. The columella-extracolumella system effectively transmits the mechanical vibrations from the eardrums to the inner ear. In the human middle-ear, the same function is performed by the bones *malleus*, *incus* and *stapes*, which are collectively known as the ossicles.

For low frequencies (below 4kHz), the extracolumella (or more accurately, the inferior process of the extracolumella) moves as a completely stiff bar. It was shown by Manley [3] that the extracolumella begins to flex at higher frequencies - this is illustrated in fig. 2.3. This is partly responsible for the poor high-frequency response of gecko middle ears -



(a) The previous geometric representation of the ICE model.



(b) The representation of the new model.

Figure 2.2: The bold arrows represent the direction conventions along the cylinder's axis. The new model is represented by a cylinder of radius a_{cyl} and length L closed at both ends by sectoral membrane of radius a_{tym} . The darkly shaded region corresponds to the extracolumella (described in Sec. 2.1.2).

a feature also observed in other non-mammalian vertebrates. The reason for this is that, due to the flection some energy is lost and not transferred to the columella.

Tympanic Membrane

The extracolumella applies a significant mechanical load on the tympanum and thereby precludes its treatment as a freely vibrating membrane. Furthermore, the contact surface of the malleus on the human eardrum is more or less symmetric whereas the extracolumella is attached asymmetrically. This has important physical consequences - especially in the observed vibration patterns of the membrane.

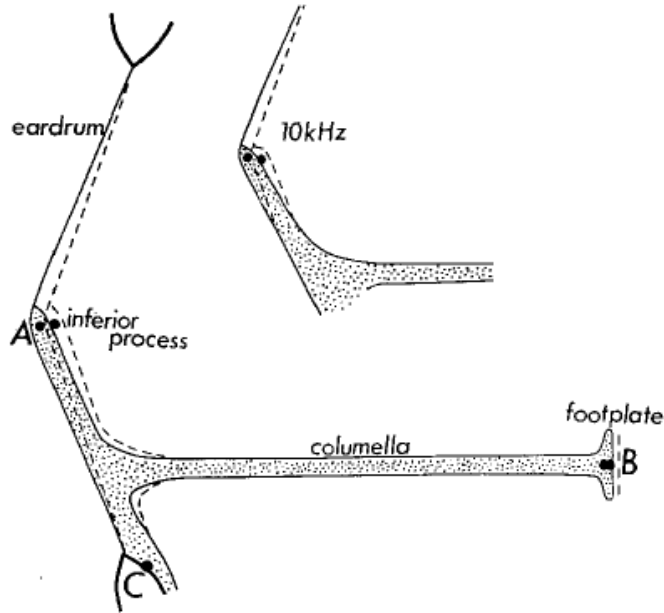


Figure 2.3: Operation of the middle ear lever in geckos reproduced from [3]. The inferior process of the extracolumella (A-C) hinges at point C at low frequencies. Also shown is the flection of the inferior process of the extracolumella.

In the previous treatment of the ICE model, the tympanum was modelled as a clamped circular membrane with assymetrically attached sectoral load between $-\beta < \phi < \beta$ ([2]). This manifests itself as an additional boundary condition at $\phi = \beta$ and $\phi = -\beta$ which has to be satisfied via a numerical approximation. While this method has the advantage of being able to accurately reproduce the complex vibration patterns of the eardrum, it does not lend itself well to an analytical treatment of the coupled system.

In our study, we will follow a slightly different path. The tympanic membrane will be modelled as a rigidly clamped sectoral membrane. This means that in addition to the radial boundary at a_{tym} , we have a new set of boundaries at $\phi = \beta$ and $\phi = 2\pi - \beta$ where the membrane vibration is set to zero. This is illustrated in 2.4. The membrane material will be assumed to be linear-elastic. As before, the equations describing the vibrations of the membrane will consequently be linear 2nd-order PDE's.

At this point we should note that we have effectively set the mass of the extracolumella to infinity. Thereby, its motion has been neglected altogether. While this may seem counterintuitive at first, we will later see that this assumption, while simplifying the problem analytically, has little effect on the physical phenomenon of interest, viz. the coupling between the eardrums and the amplification of hearing cues. This will be discussed in-depth in Chapter 3.

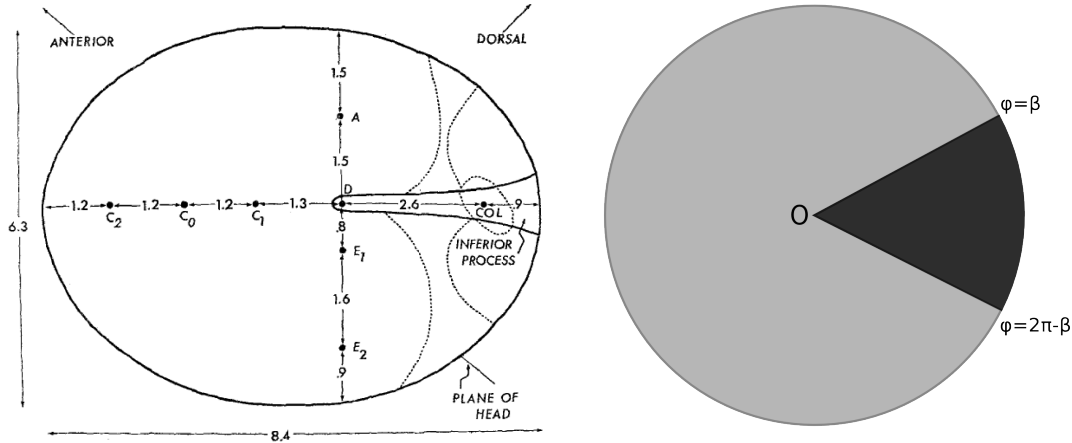


Figure 2.4: Left: Sketch of the eardrum of a Tokay gecko as seen from the outside taken from Manley, [17]. “COL” is the approximate position opposite the extracolumella insertion. The dots indicate the positions for measurements and will be discussed briefly in the next chapter. Dimensions in millimeters. Right: Our model for the loaded tympanic membrane. The lightly shaded region is modelled as a linear elastic membrane whereas the darkly shaded region ($\beta < \phi < 2\pi - \beta$) represents the contact surface of the extracolumella and the membrane. β corresponds to the breadth of the extracolumella and is estimated from anatomical data.

2.1.3 Head Model and External Sound Input

In realistic environments the acoustic fields experienced by animals are often very complex. In addition to sound waves radiated directly from one or more sources in general, they also involve waves reflected from objects in their immediate neighbourhood. Higher animals such as humans possess the neural power to carry out the sophisticated signal processing needed to derive useful information from these signals. Simpler animals like geckos respond to simpler cues - usually the direct field from the nearest or strongest source.

We can therefore model our incoming wave as the simple case of an incident plane wave of a certain frequency. This input is specified in terms of its intensity, frequency and direction. Such a stimulus can be generated in an anechoic chamber from loudspeakers which are placed at a distance from the animal that is large compared to the animal’s size and the wavelength of the sound involved. Such experimental-setups are more thoroughly described by Christensen-Dalsgaard and Manley ([4], [5]) and Christensen-Dalsgaard, Tang and Carr ([6]).

The amplitude of the sound pressure incident on both ears can be taken as uniform in over the surface of the membrane. The spatial variation can be safely neglected because the typical eardrum is less than 5mm in diameter whereas the smallest sound wavelengths in the hearing range of the larger lizards (eg. Tokay gecko) is around 70mm (4000 Hz) and is around 50mm (7000 Hz) for the smaller lizards (eg. Hemidactylus). In other experiments, a similar stimulus has also been provided by means of a headphone sealed to the ear ([7]).

In general a the sound on the other side of the head will differ in phase as well as

amplitude. This is a result of the diffraction of sound around the head and body of the animal. The exact variation depends on the size of the animal and the frequency of the incident wave. Due to the typically small head size of geckos, the amplitude variation (known as shadowing) is negligible ([8]). The phase difference, although small compared to those in larger animals, cannot be neglected. We can therefore consider the sound wave with angular frequency ω to have a constant (pressure) amplitude p on the head.

In the earlier ICE model, the effect of diffraction on the phase difference was neglected as well. The phase difference is found directly from the phase difference Δ as shown in fig. 2.5. As a result, the sound pressure inputs at both ears is given by,

$$p_0 = pe^{j\omega t} e^{-k\Delta/2}, \quad p_L = pe^{j\omega t} e^{k\Delta/2}, \quad \Delta = L \sin \theta. \quad (2.2)$$

We note that in defining the input in this way, we've emphasized the symmetry of the system. The ear closer to the sound source is referred to as the *ipsilateral* ear and is denoted by a subscript 0 and the one further away from the source is referred to as the *contralateral* ear and is denoted by a subscript L . Subsequently, unless otherwise specified, the subscripts 0 and L will correspond to the ipsi- and contralateral ears respectively. We

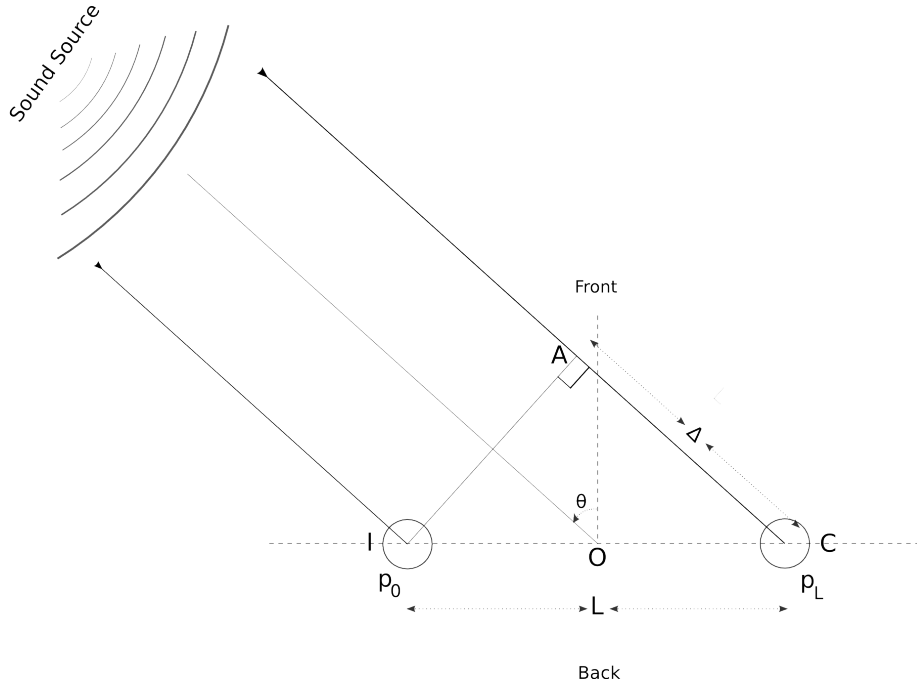


Figure 2.5: The previous acoustic head model for geckos. The extra distance travelled by the sound wave to reach the contralateral ear is denoted by Δ .

have also chosen a coordinate system relative to the *median-sagittal* plane or the head midline of the animal and θ gives the angle of incidence of this sound wave relative to this plane. For more complex auditory systems we would require two angles (θ, ϕ) to describe the three-dimensional system but in our analysis this is unnecessary. For the animals we

are concerned with, i.e. geckos, the natural predators and prey are usually present on the same plane as the animal and our assumption is therefore reasonable.

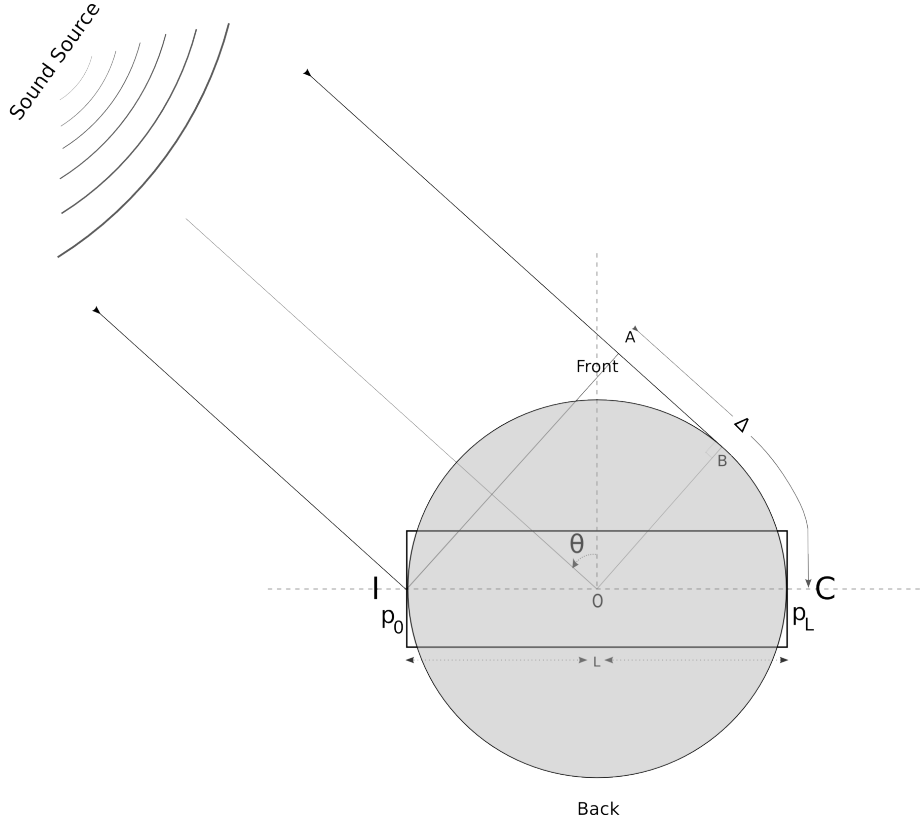


Figure 2.6: The acoustic head model for geckos. The rectangular outline is the internal cavity. As before, the extra distance travelled by the sound wave to reach the contralateral ear is given by Δ . In this case, however, we have accounted for the influence of diffraction around the head on the phase difference between the inputs to both ears.

In our model we model the head as a sphere with a diameter equal to the interaural separation. As a result the sound has to travel around the head in order to reach the contralateral ear resulting in a longer path. The frequency domain solution for the diffraction of sound around a sphere was obtained by Lord Rayleigh at the end of the 19th century ([9],[10]). The expressions are greatly simplified at low frequencies and the phase difference is simply increased by a factor of 1.5 (i.e. $\Delta_{new} = 1.5\Delta$). The new model is illustrated in Fig. 2.6.

2.2 Derivation of the Model

We will now use the previously described physical model to derive the main expressions of interest in the ICE model - the membrane vibration profiles, the ipsi- and contralateral filters and the cavity pressure distribution. We will thus find an expression for the pressure

distribution in the cylindrical cavity and for the membrane vibrations subject to an external stimulus. After applying the appropriate boundary conditions to relate the membrane vibrations to the internal pressure, we will find the expression for the membrane vibrations as a function of direction and frequency.

We will start in Sec. 2.2.1 by finding a general solution to a 2nd-order PDE - the 3D wave equation - that describes the pressure distribution inside the cylindrical cavity. In this section we will introduce the main boundary condition the pressure will be subject to - the “no-penetration” boundary condition. This is a physical requirement that results from the fact that the air inside the cavity does not penetrate a solid boundary.

In Sec. 2.2.2 we will solve for the vibrations of the tympanic membranes. As an example, we will find an expression for the free and periodically driven vibrations of a circular membrane. Using the methods developed in this section, we will solve for the vibrations of a sectoral membrane - which, as we have already discussed, models the loaded tympanum. The final expression will correspond to the steady-state vibrations of a linear elastic membrane. As we neglect the transient response of the membrane, we will also discuss the circumstances under which this is justified.

In Sec. 2.2.3 we will conclude by using our knowledge to solve for the vibration of the fully coupled system. In this section we will proceed by applying the velocity boundary condition at either end of the cylinder. In order to help with our analysis, we will present a simplification scheme for this boundary condition. We will end this section by defining the ipsi- and contralateral filters. The final expressions that give us the vibrations of the tympanic membranes as a function of the external pressure with the influence of the internal cavity encoded in the ipsi- and contralateral filters. We have listed the main parameters and functions used in our analysis (including the geometry parameters) in Tables 2.1 and 2.2.

Table 2.1: Functions and Parameters used in the ICE Model

θ	Direction of the sound source with respect to the head midline.
ω	Angular frequency of the incoming sound wave.
k	Wavenumber $k = \omega/c$ with $c = 343\text{m/s}$ being the speed of sound.
p	Pressure amplitude of the incoming sound wave.
Δ	Phase difference between the sound wave reaching the contra- and ipsilateral ear.
$p_{0/L}$	Sound pressure on the ipsi- ($x = 0$) and contralateral ($x = L$) ears respectively.
(x, r, ϕ)	Cylindrical polar coordinates with x being the axial direction.
L	Interaural separation and length of cylinder.
a_{cyl}	Radius of cylinder.
a_{tym}	Radius of tympanum.
$\beta < \phi < 2\pi - \beta$	Extent of the vibrating part of the membrane. The rest of the circle corresponds to the extracolumellar footplate.
V_0	Volume of the cavity.

Table 2.2: Functions and Parameters used in the ICE Model contd.

J_q	Order q Bessel function of the first kind.
μ_{qs}, ν_{qs}	Respectively - s^{th} zero and s^{th} extremum of the above Bessel function.
$f_{qs}(x, r, \phi)$	Orthogonal modes for the pressure distribution inside the mouth cavity.
ζ_{qs}	Wavenumber of the above modes in the x -direction.
$p(x, r, \phi; t)$	Pressure distribution inside the mouth cavity.
$v_x(x, r, \phi; t)$	Velocity function inside the mouth cavity.
$u_{mn}(r, \phi; t)$	Eigenmodes of the membrane displacement function.
ω_{mn}	Eigenfrequency of the above eigenmodes.
Q	Quality factor of the membrane.
$\Psi(r, \phi; t)$	Driving pressure on the membrane.
$u_{0/L}(r, \phi; t)$	Membrane displacement function.
$S^{0/L}(t)$	Total membrane displacement.
$G_{ipsi}(r, \phi)$	Ipsilateral filter.
$G_{contra}(r, \phi)$	Contralateral filter.

2.2.1 Internal Cavity

We assume that the air inside the cavity obeys linear acoustics (cf. acoustic textbooks such as [11, p. 313] and [12, p. 247]). This means that the air moves due to pressure $p(x, r, \phi; t)$ whose distribution inside the cavity is given by the 3D acoustic wave-equation in cylindrical polar coordinates,

$$\frac{1}{c^2} \frac{\partial^2 p(x, r, \phi, t)}{\partial t^2} = \frac{1}{r} \frac{\partial}{\partial r} \left(r \frac{\partial p(x, r, \phi, t)}{\partial r} \right) + \frac{1}{r^2} \frac{\partial p(x, r, \phi, t)}{\partial \phi^2} + \frac{\partial p(x, r, \phi, t)}{\partial x^2} \quad (2.3)$$

where c is the sound propagation velocity. The complete solution must take into account the boundary conditions at and within the cavity walls and the ones at the air-membrane interface. We also note that the above equation implies that the animal's mouth is closed, which is typical for a waiting animal. In order to solve (2.3) for a particular frequency f (angular frequency $\omega = 2\pi f$), we use the following separation ansatz

$$p(x, r, \phi, t) = f(x)g(r)h(\phi)e^{j\omega t} \quad (2.4)$$

which after substitution into the acoustic wave-equation leads to,

$$\begin{aligned} k^2 f(x)g(r)h(\phi) + f(x)h(\phi) \left[\frac{\partial^2 g(r)}{\partial r^2} + \frac{1}{r} \frac{\partial g(r)}{\partial r} \right] \\ + f(x)g(r) \frac{1}{r^2} \frac{\partial h(\phi)}{\partial \phi} + \frac{\partial^2 f(x)}{\partial x^2} = 0 \end{aligned} \quad (2.5)$$

with $k := \omega/c$. This results in the following set of separated ODE's,

$$\frac{d^2 f(x)}{dx^2} + \zeta^2 f(x) = 0 \quad (2.6)$$

$$\frac{d^2 h(\phi)}{d\phi^2} + q^2 h(\phi) = 0 \quad (2.7)$$

$$\frac{\partial^2 g(r)}{\partial r^2} + \frac{1}{r} \frac{\partial g(r)}{\partial r} + \left[\underbrace{(k^2 - \zeta^2)}_{=: \nu^2} - \frac{q^2}{r^2} \right] g(r) = 0 \quad (2.8)$$

with separation constants q and ζ . The last equation is the Bessel differential equation [13, p. 313] and its general solution is given by,

$$g(r) = C_{qs} J_q(\nu r) + D_{qs} Y_q(\nu r). \quad (2.9)$$

J_q and Y_q are the order- q Bessel functions of the first and second kind respectively. The Bessel function of the second kind can be ignored as it diverges at $r = 0$. The solutions to the separated equations are therefore given by,

$$f(x) = e^{\pm \zeta x}, \quad h(\phi) = e^{\pm j\phi}, \quad \text{and} \quad g(r) = J_q(\nu r) \quad (2.10)$$

with a specific solution to (2.3) given by,

$$p(x, r, \phi; t) = [(A^+ e^{jq\phi} + A^- e^{-jq\phi}) e^{j\zeta x} + (B^+ e^{jq\phi} + B^- e^{-jq\phi}) e^{-j\zeta x}] J_q(\nu r) e^{j\omega t}. \quad (2.11)$$

The coefficients A^\pm , B^\pm , q , ζ and ν will be subsequently determined by the boundary conditions.

In general, the time component of the pressure also has a *backward-moving* component, i.e. $e^{-j\omega t}$. By making the ansatz in (2.4), we have implicitly made use of the fact that the form of the input constrains the pressure to only have a *forward-moving* component, i.e. $e^{j\omega t}$.

Pressure Boundary Conditions

There are three sets of boundary conditions -

- Continuity and smoothness in ϕ which is equivalent to $h(0) = h(2\pi)$ and $h'(0) = h'(2\pi)$ where, $h' = dh/d\phi$.

- Vanishing of the normal derivative at the cavity walls - $g'(a_C) = 0$ (a_C is the radius of the cylinder).
- Equating the membrane velocity to the velocity function at the membrane boundaries (to be discussed in the next section).

The first set of requirements is obvious. This reduces (2.11) to

$$p(x, r, \phi; t) = [Ae^{j\zeta x} + Be^{-j\zeta x}] \cos q\phi J_q(\nu r) e^{j\omega t}. \quad (2.12)$$

With q constrained to be an integer.

The second and third are a result of the so called “no-penetration” boundary-condition of fluid-mechanics. It arises from the fact that the cavity wall is an impermeable boundary. This translates into the requirement that the normal velocity function should vanish ([14, p. 111]). The velocity function (\mathbf{v}) is related to the pressure by,

$$-\rho \frac{\partial \mathbf{v}}{\partial t} = \nabla p \quad (2.13)$$

At the cylindrical cavity wall, the normal velocity is in the radial direction. Substituting the expression for pressure in (2.11) in the above equation leads to a Neumann boundary condition for the pressure,

$$\begin{aligned} v_r &= -\frac{1}{j\rho\omega} \left. \frac{\partial p(x, r, \phi; t)}{\partial r} \right|_{r=a_C} = 0 \\ &\Rightarrow \left. \frac{\partial J_q(\nu r)}{\partial r} \right|_{r=a_C} = 0 \end{aligned} \quad (2.14)$$

This constrains ν to a discrete set of values which correspond to the local minima and maxima of J_q . We can therefore index ν by q and $s = 0, 1, 2, 3, \dots$ with $\nu_{qs} = z_{qs}/a_C$: z_{qs} being the s^{th} extremum of the order- q Bessel function of the first kind. This results in a discrete set of modes that satisfy (2.3) which are given by,

$$p_{qs}(x, r, \phi; t) = [A_{qs}e^{j\zeta_{qs}x} + B_{qs}e^{-j\zeta_{qs}x}] f_{qs}(r, \phi) e^{j\omega t} \quad (2.15)$$

where we have added the subscripts q and s to ζ and denoted the (r, ϕ) part of (2.12) by $f_{qs}(r, \phi)$. Effectively, the modes are 3D waves propagating with wave numbers ζ_{qs} in the x -direction and ν_{qs} in the radial direction. The first of these modes (corresponding to $q = 0, s = 0$) is of particular importance. Since the first maximum of J_0 occurs at $r = 0$, we have $\nu_{00} = 0$. This leads to the first mode being a plane-wave which is constant in r and ϕ and only varies in x .

A very useful property of the above modes is their orthogonality, i.e.

$$\int_{\Omega} dV p_{q_1 s_1} p_{q_2 s_2} = 0, \text{ if } q_1 \neq q_2 \text{ or } s_1 \neq s_2 \quad (2.16)$$

the integral is over the volume of the cylinder. This is a consequence of the fact that for different q 's the cosine parts of the modes are orthogonal whereas for a given q the Bessel parts are orthogonal for different s 's or expressed as an equation,

$$\int dS f_{q_1 s_1} f_{q_2 s_2} = 0, \quad q_1 \neq q_2 \text{ or } s_1 \neq s_2 \quad (2.17)$$

where $dS = r dr d\phi$ and the integral being taken over the disk of radius a_C . We can therefore write the general solution to (2.3) as a linear combination of the orthogonal modes given in (2.15),

$$p(x, r, \phi; t) = \sum_{q=0}^{\infty} \sum_{s=0}^{\infty} (A_{qs} e^{j\zeta_{qs} x} + B_{qs} e^{-j\zeta_{qs} x}) f_{qs}(r, \phi) e^{j\omega t} \quad (2.18)$$

The remaining coefficients, A_{qs} and B_{qs} , will be determined by equating the velocity function to the membrane velocity at both ends of the cylinder. To do so, we will first need to find an expression for the membrane vibrations - as we will in the following section.

2.2.2 Vibration of the Membrane

As a preliminary exercise, we will first derive expressions for the free and force-driven vibrations of a circular membrane. We will then use our results to move on to the sectoral membrane which corresponds to the tympanum loaded by the extracolumella. This corresponds to the approximating the extracolumella to have infinite mass.

Circular Membrane

The equation of motion for the vibration of a rigidly clamped circular membrane of radius a_M solves for the membrane displacement u at a point (r, ϕ) with $r < a$ and $0 < \phi < 2\pi$. It is given by,

$$\begin{aligned} -\frac{\partial^2 u(r, \phi; t)}{\partial t^2} - 2\alpha \frac{\partial u(r, \phi; t)}{\partial t} + c_M^2 \left[\frac{1}{r} \frac{\partial}{\partial r} \left(r \frac{\partial u(r, \phi, t)}{\partial r} \right) + \frac{1}{r^2} \frac{\partial^2 u(r, \phi, t)}{\partial \phi^2} \right] \\ = \frac{1}{\rho_M d} \Psi(r, \phi; t) \end{aligned} \quad (2.19)$$

subject to the boundary condition $u(r, \phi; t)|_{r=a_M} = 0$. We've defined the following membrane material properties,

- c_M - propagation speed of vibrations.
- $\alpha(> 0)$ - the damping coefficient.
- ρ_M - density.
- d - thickness.

$\Psi(r, \phi; t)$ is the pressure on the membrane surface at (r, ϕ) . In our discussion we are only concerned with periodic and uniform pressure acting on the membrane surface. As we have already stated in Sec. 2.1.3, the small size of the membrane with respect to the sound wavelength, justifies the spatial uniformity of our input.

Free Vibrations

Undamped Membrane: We first determine the eigenmodes of an undamped circular membrane by solving (2.19) for $\alpha = 0$, $\Psi = 0$ (the resultant equation is better known as the 2D Helmholtz equation, cf. [15, p. 187]). Just as we did in (2.4), we do this by making a separation ansatz ,

$$u(r, \phi; t) = f(r)g(\phi)h(t) \quad (2.20)$$

This gives us the following set of equations

$$\frac{\partial^2 f(r)}{\partial r^2} + \frac{1}{r} \frac{\partial f(r)}{\partial r} + \left[\mu^2 - \frac{m^2}{r^2} \right] f(r) = 0 \quad (2.21)$$

$$\frac{d^2 g(\phi)}{d\phi^2} + m^2 g(\phi) = 0 \quad (2.22)$$

$$\frac{d^2 h(t)}{dt^2} + c_M^2 \mu^2 h(t) = 0 \quad (2.23)$$

with separation constants μ and m . The solution of the first of these equations should already be familiar to us from the previous section - $J_m(\mu r)$, the order- m Bessel function of the first kind. The boundary conditions in ϕ direction remain the same resulting in,

$$u(r, \phi; t) = [(M^+ e^{jm\phi} + M^- e^{-jm\phi}) e^{jc_M \mu t} + (N^+ e^{jm\phi} + N^- e^{-jm\phi}) e^{-jc_M \mu t}] J_m(\mu r) \quad (2.24)$$

Unlike in the case of the internal cavity, we require u to vanish at the boundary so we have a Dirichlet boundary condition which effectively requires: $J_m(\mu a_M) = 0$. This constrains μ to a discrete set of values which correspond to the zeros of J_m . The eigenmodes of a the circular membrane are therefore given by,

$$u_{mn}(r, \phi; t) = [(M_{mn}^+ e^{jm\phi} + M_{mn}^- e^{-jm\phi}) e^{j\omega_{mn} t} + (N_{mn}^+ e^{jm\phi} + N_{mn}^- e^{-jm\phi}) e^{-j\omega_{mn} t}] J_m(\mu_{mn} r) \quad (2.25)$$

where $\mu_{mn} = z_{mn}/a_M$, z_{mn} being the n^{th} zero of J_m and, $\omega_{mn} = c_M \mu_{mn}$ is the eigenfrequency of the (m, n) eigenmode. At this point m can take any positive real value – a fact that will help us solve the sectoral membrane problem. However, in the case of a full circular membrane – as in the case of the pressure inside a cylindrical cavity – requirements of continuity and smoothness in ϕ reduce (2.25) to,

$$u_{mn}(r, \phi; t) = \cos m\phi J_m(\mu_{mn} r) [M_{mn} e^{j\omega_{mn} t} + N_{mn} e^{-j\omega_{mn} t}] \quad (2.26)$$

with $m = 0, 1, 2, \dots$ with the (m, n) eigenmodes forming an orthogonal set. For later convenience we denote the spatial part of the above mode by $u_{mn}(r, \phi)$. The first few of these modes are plotted in 2.7.

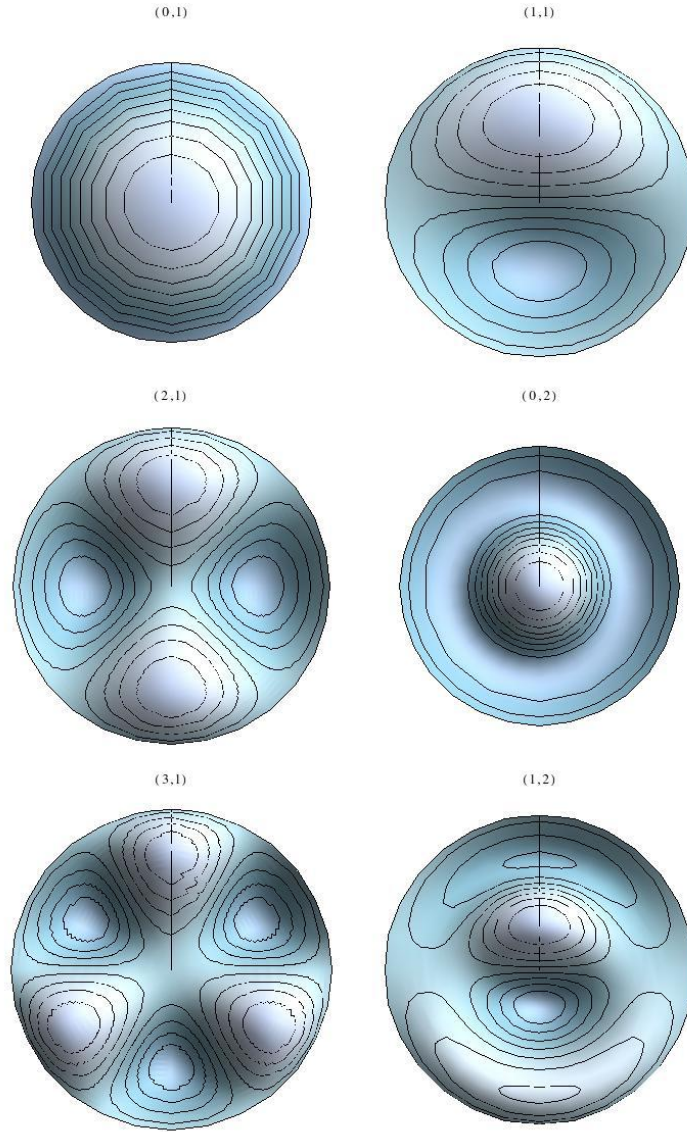


Figure 2.7: Eigenmodes of a full circular membrane. The eigenfrequency increases from left to right.

We note that unlike in the case of the internal cavity, the free membrane has components that are both forward- and backward-moving in time. The presence of a driving force, however, will result in simpler expressions. This will be discussed in more detail in the next chapter where we compare our model with experimental data.

Damped Membrane: For a damped membrane, i.e. $\alpha \neq 0$, the spatial part of the above eigenmodes remains the same. The form of the time-dependent part is given by the

solution of the equation,

$$\frac{d^2 h_{mn}(t)}{dt^2} + 2\alpha \frac{dh_{mn}(t)}{dt} + \omega_{mn}^2 h_{mn}(t) = 0. \quad (2.27)$$

Assuming h_{mn} takes the form $e^{j\tilde{\omega}_{mn}}$ leads to a quadratic equation with solutions,

$$\tilde{\omega}_{mn} = j\alpha \pm \omega_{mn}^* \quad (2.28)$$

$$\omega_{mn}^* = \sqrt{\alpha^2 + \omega_{mn}^2} \quad (2.29)$$

We require the membrane displacement to remain finite as $t \rightarrow \infty$. We can therefore neglect the $e^{-j\tilde{\omega}_{mn}}$ terms leading to,

$$\tilde{u}_{mn}(r, \phi; t) = \cos m\phi J_m(\mu_{mn}r) [M_{mn}e^{j\omega_{mn}^* t} + N_{mn}e^{-j\omega_{mn}^* t}] e^{-\alpha t} \quad (2.30)$$

The general solution is given by a linear combination of the above and the coefficients are determined by initial conditions – for example, membrane displacement and velocity at $t = 0$.

Forced Vibrations

For a periodically driven membrane, there are two components of the full solution for forced vibrations. The first of these is the steady state solution which oscillates with the same frequency as the input and does not depend on the initial conditions - u_{ss} . The second of these is the transient solution that depends on the initial conditions but not on the driving pressure - u_t .

Steady State Solution: The steady state solution is expressed as a linear combination of the spatial part of the above eigenmodes and is given by,

$$u_{ss}(r, \phi; t) = \sum_{m=0}^{\infty} \sum_{n=1}^{\infty} C_{mn} \cos m\phi J_m(\mu_{mn}r) e^{j\omega t}. \quad (2.31)$$

Substituting this expression in (2.19) with $\Psi = pe^{j\omega t}$ gives,

$$\sum_{m=0}^{\infty} \sum_{n=1}^{\infty} \Omega_{mn} C_{mn} \cos m\phi J_m(\mu_{mn}r) e^{j\omega t} = pe^{j\omega t} \quad (2.32)$$

$$\text{where, } \Omega_{mn} = \rho_M d [(\omega^2 - \omega_{mn}^2 n) - 2j\alpha\omega]. \quad (2.33)$$

Using the orthogonality of the eigenmodes, the coefficients C_{mn} can be calculated,

$$C_{mn} = \frac{p \int dS u_{mn}}{\Omega_{mn} \int dS u_{mn}^2} \quad (2.34)$$

with the integral this time being taken over the circular disk of radius a_M .

Transient Solution: The transient solution is effectively a solution of the free damped membrane, i.e. a linear combination of the eigenmodes given in (2.30). Therefore,

$$u_t(r, \phi; t) = \sum_{m=0}^{\infty} \sum_{n=1}^{\infty} \cos m\phi J_m(\mu_{mn}r) [M_{mn} e^{j\omega_{mn}^* t} + N_{mn} e^{-j\omega_{mn}^* t}] e^{-\alpha t}. \quad (2.35)$$

The complete solution is given by $u = u_t + u_{ss}$ and the coefficients M_{mn} and N_{mn} are determined by the initial conditions (at $t = 0$).

Steady State Approximation: The damping coefficient α is usually given in terms of the membrane fundamental frequency and a quality factor Q as $\alpha = \omega_{01}/2Q$. For the tympani we will be concerned with we have $Q \sim 1.2$ which results in damping coefficients that are around $4000s^{-1}$ for the larger lizards and around $8000s^{-1}$ for the smaller ones. Due to this and the exponential decay of the transient vibration amplitude, we can safely assume that within a few time-periods the steady-state vibrations dominate the solution of the forced membrane. For this reason, we will subsequently confine our discussion to only the steady state vibrations of the membrane.

Sectoral Membrane

The eigenmodes of the sectoral membrane proceeds from (2.25) onwards. We now have a new set of boundary conditions in ϕ . The extracolumella is modelled as a triangular plate of infinite mass which constrains the membrane displacement to go to zero at $\phi = \beta$ and $\phi = 2\pi - \beta$. This results in the following set of eigenmodes,

$$u_{mn}(r, \phi; t) = \sin \kappa(\phi - \beta) J_\kappa(\mu_{mn}r) [M_{mn} e^{j\omega_{mn} t} + N_{mn} e^{-j\omega_{mn} t}] \quad (2.36)$$

where $\kappa[m] = \frac{m\pi}{2(\pi-\beta)}$, $m = 1, 2, 3, \dots$. We see that the r part of the above mode is given by the order- κ Bessel function of the first kind; μ_{mn} being its n^{th} zero, as before. The solution for the damped membrane follows in an identical way. It is apparent from the form of the above modes that, unlike in the case of the circular membrane eigenmodes, these modes are no longer circularly symmetric. We plot the first few of these modes in 2.8. The solution for forced membrane vibrations follows in the same way as in the circular membrane case. The vibrations of a sectoral membrane are discussed in more detail in [16, p. 87]. As discussed earlier, the sectoral shape of the membrane has important physical consequences and captures the complex vibration patterns of a realistic membrane. This will be discussed in the next chapter.

2.2.3 Vibration of Coupled Membranes

With our current knowledge, we can move on to the main part of the chapter - the vibration of coupled membranes. It is convenient to first write down the main equations of the system

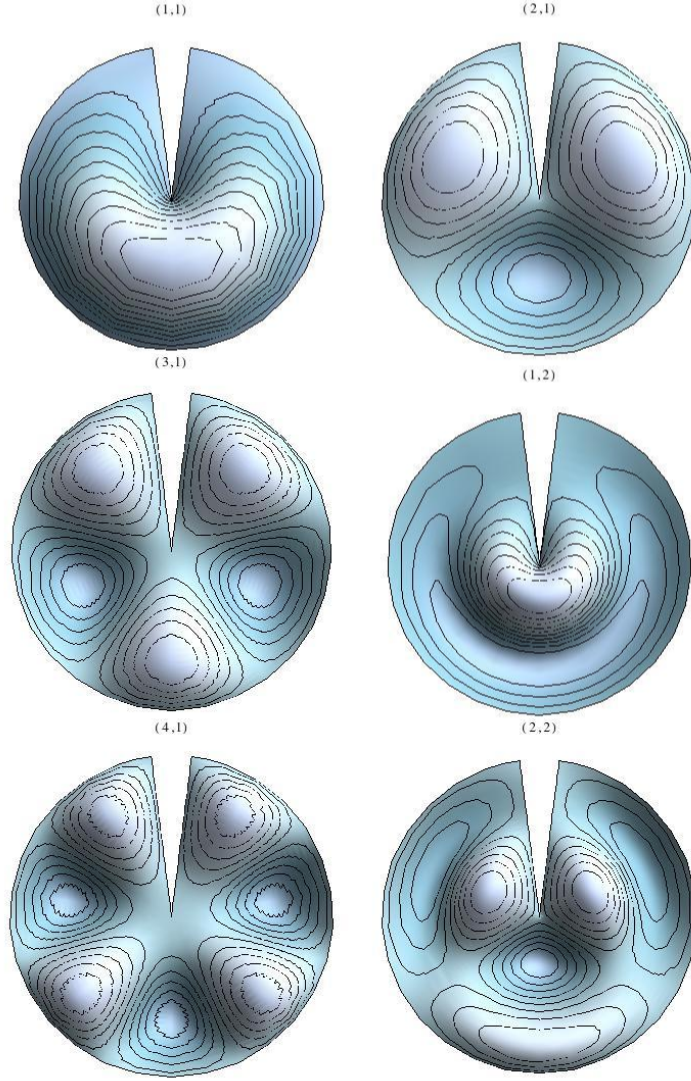


Figure 2.8: Eigenmodes of a sectoral membrane with $\beta = \pi/25$. The eigenfrequency increases from left to right.

based on our previously derived expressions. The vibrations of the membranes is given by,

$$u_{0/L}(r, \phi; t) = \sum_{m=0}^{\infty} \sum_{n=1}^{\infty} \Omega_{mn} C_{mn}^{0/L} u_{mn}(r, \phi) e^{j\omega t} = p_{0/L} e^{j\omega t} - p(0/L, r, \phi; t) \quad (2.37)$$

where 0 and L denote the ipsi- and contra-lateral membranes respectively and the cavity pressure distribution, $p(x, r, \phi; t)$, is given by (2.18). The above equation is only valid on the membrane surface i.e., for $r < a_{typ}$ and $\beta < \phi < 2\pi - \beta$.

As discussed in 2.2.1, the internal cavity pressure satisfies the no-penetration condition at solid boundaries. This means that at both ends of the cylinder, we equate the velocity profile of air to the velocity profile of the circular surface including the membrane. This is

because the membrane diameter is smaller than the cylinder diameter. As a result, we will have to set the air-particle velocity to zero for $r > a_{tym}$. Since the membrane displacement is only in the x -direction, we only need to calculate the same component of the velocity. Using the relation (2.13) we get,

$$v_x(x, r, \phi; t) = -\frac{1}{\rho\omega} \sum_{q=0}^{\infty} \sum_{s=0}^{\infty} \zeta_{qs} (A_{qs} e^{j\zeta_{qs}x} - B_{qs} e^{-j\zeta_{qs}x}) f_{qs}(r, \phi) e^{j\omega t} \quad (2.38)$$

and the exact boundary conditions are given by,

$$j\omega U_0 = v_x(0, r, \phi; t) \quad (2.39)$$

$$j\omega U_L = -v_x(L, r, \phi; t) \quad (2.40)$$

where we've used the direction conventions described in 2.1 and made the following definition,

$$U_{0/L} = \begin{cases} u_{0/L}, & 0 < r < a_{tym} \text{ and } \beta < \phi < 2\pi - \beta \\ 0, & \text{otherwise} \end{cases} . \quad (2.41)$$

This in order to ensure that the boundary condition is satisfied over either end of the cylinder and not just over the membrane surface.

Approximate Boundary Condition

As previously stated, the exact boundary condition would entail setting the velocity function to be exactly equal to the membrane displacement velocity. At this point, it is important to note that the internal cavity eigenmodes are **not** orthogonal to the membrane eigenmodes in general¹. This means that every membrane eigenmode couples with every cavity eigenmode and that each of the coefficients A_{qs} and B_{qs} will be given by an infinite linear combination of the coefficients $C_{mn}^{0/L}$.

The first step in overcoming this problem is to rewrite the left-hand sides of the boundary conditions given in (2.39) and (2.40). We first expand U_0 and U_L in the orthogonal basis of the functions f_{qs} ,

$$U_{0/L}(r, \phi; t) = \sum_{q=0}^{\infty} \sum_{s=0}^{\infty} S_{qs}^{0/L} f_{qs}(r, \phi) e^{j\omega t} \quad (2.42)$$

$$\text{where, } S_{qs}^{0/L} = \frac{\int dS U^{0/L} f_{qs}(r, \phi)}{\int dS f_{qs}^2(r, \phi)} \quad (2.43)$$

We now have an expansion that approximates the boundary condition with increasing accuracy. After choosing an appropriate cutoff for the expansion we can substitute this expression in place of $U_{0/L}$ in (2.39) and (2.40). In fact, this cutoff in the boundary

¹This would also be true if we had full circular membranes on either end of the cylinder. In this case we would have the added simplification that only the circularly symmetric cavity eigenmodes will be activated.

condition expansion results in an identical cutoff in the pressure expansion - a direct result of the orthogonality of the pressure modes.

We will now illustrate a solution to the problem by solving the problem with the zeroeth order boundary conditions. In the end, it will turn out that for our purposes the zeroeth order, i.e. the $(0, 0)$ mode is sufficient as higher modes only have a significant contribution at frequencies well above the hearing range of geckos. For example, the wavenumber of the $(1, 1)$ mode is above 33kHz for the cylindrical cavity corresponding to the house gecko and above 15kHz for the one corresponding to the Tokay gecko. The parameters used to derive these quantities will be discussed in the next chapter. We can therefore write the approximate boundary conditions to zeroeth order as,

$$\rho\omega^2 S^0 = \sum_{q=0}^{\infty} \sum_{s=0}^{\infty} j\zeta_{qs} (A_{qs} - B_{qs}) f_{qs}(r, \phi) \quad (2.44)$$

$$\rho\omega^2 S^L = - \sum_{q=0}^{\infty} \sum_{s=0}^{\infty} j\zeta_{qs} (A_{qs} e^{j\zeta_{qs} L} - B_{qs} e^{-j\zeta_{qs} L}) f_{qs}(r, \phi) \quad (2.45)$$

As shown in Sec. 2.2.1, the $(0, 0)$ mode only varies in the x -direciton. As a result, the left-hand sides of the above equation are nothing but the average displacement of the membrane surface given by,

$$S^{0/L} = \frac{\int dS U^{0/L}(r, \phi)}{\pi a_{cyl}^2}. \quad (2.46)$$

We have also omitted the “ qs ” subscript from $S^{0/L}$. Given the external parameters and boundary conditions, it only depends on time. We have effectively approximated the surfaces at 0 and L (including the membranes) by pistons moving with the average velocity of the total surface.

Given these boundary conditions, it is straightforward to calculate the coefficients A_{qs} and B_{qs} in terms of $S_{0/L}$. To do this we need to make use of the orthogonality relation given in (2.17). We do this by multiplying both sides of (2.44) and (2.45) by $f_{qs}(r, \phi)$ and integrate over the circular surfaces at either end of the cylinder. This results in a system of two linear equations for each pair of A_{qs} and B_{qs} ,

$$A_{qs} - B_{qs} = L_{qs} \rho \omega^2 S^0 \quad (2.47)$$

$$A_{qs} e^{j\zeta_{qs} L} - B_{qs} e^{-j\zeta_{qs} L} = -L_{qs} \rho \omega^2 S^L \quad (2.48)$$

$$\text{where, } L_{qs} = \frac{\int dS f_{qs}(r, \phi)}{j\zeta_{qs} \int dS f_{qs}^2(r, \phi)}$$

We now make use of the property of the pressure modes that $f_{qs}(r, \phi)$ integrates to 0 unless $q = 0$ and $s = 0$. For $q = 0$ this is a consequence of the Bessel functions integrating to zero while for $q \geq 1$ this is due to the more obvious fact that the integral of the cosine function from 0 to 2π is zero. As a result we have $A_{qs} = B_{qs} = 0$ for all modes except the $(0, 0)$ mode. In other words, the zeroeth-order boundary condition only supports

plane wave modes inside the cavity. We will subsequently omit the subscripts “00” for these coefficients. From the above linear equations, they are given in terms of the total membrane displacement as,

$$A = \frac{\rho\omega^2}{2k \sin kL} (S^0 e^{-jkL} + S^L), \quad B = \frac{\rho\omega^2}{2k \sin kL} (S^0 e^{jkL} + S^L) \quad (2.49)$$

we have also directly substituted $\zeta_{00} = k$ and simplified the expression for K_{00} in the above expressions. These coefficients can now be substituted in place of the pressure in the right-hand side of the equation (2.37) giving us,

$$\sum_{m=0}^{\infty} \sum_{n=1}^{\infty} \Omega_{mn} C_{mn}^0 u_{mn}(r, \phi) = p_0 - \frac{\rho\omega^2}{k} (S^0 \cot kL + S^L \csc kL) \quad (2.50)$$

$$\sum_{m=0}^{\infty} \sum_{n=1}^{\infty} \Omega_{mn} C_{mn}^L u_{mn}(r, \phi) = p_L - \frac{\rho\omega^2}{k} (S^0 \csc kL + S^L \cot kL) \quad (2.51)$$

where we have cancelled out the time component on both sides of the equations. Note that the right-hand sides of the above two equations are independent of the spatial (r, ϕ) coordinates.

In order to simplify the above coupled system of equations, the next step will be to take their sum and difference to obtain a new set of variables that are solutions of a pair of decoupled equations. After some algebraic manipulation, we therefore have

$$\sum_{m=0}^{\infty} \sum_{n=1}^{\infty} \Omega_{mn} C_{mn}^+ u_{mn}(r, \phi) = p_+ - \frac{\rho\omega^2}{k} S^+ \cot \frac{kL}{2} \quad (2.52)$$

$$\sum_{m=0}^{\infty} \sum_{n=1}^{\infty} \Omega_{mn} C_{mn}^- u_{mn}(r, \phi) = p_- - \frac{\rho\omega^2}{k} S^- \tan \frac{kL}{2} \quad (2.53)$$

where, $C_{mn}^+ = C_{mn}^L + C_{mn}^0$ and $C_{mn}^- = C_{mn}^L - C_{mn}^0$. The $S^{+/-}$ and $p_{+/-}$ terms are defined similarly. Now, analogous to the calculation of the coefficients for the steady state vibration in (2.32) and (2.34), we can determine the coefficients of the sum and difference vibrations in terms of the pressure and total membrane displacements. This gives us,

$$C_{mn}^+ = \left[p_+ - \frac{\rho\omega^2}{k} S^+ \cot \frac{kL}{2} \right] K_{mn} \quad (2.54)$$

$$C_{mn}^- = \left[p_- - \frac{\rho\omega^2}{k} S^- \tan \frac{kL}{2} \right] K_{mn} \quad (2.55)$$

$$\text{where, } K_{mn} = \frac{\int dS u_{mn}}{\Omega_{mn} \int dS u_{mn}^2}$$

The next step will be to multiply both sides of (2.54) and (2.55) with the integral $\int dS u_{mn}$, divide by πa_{cyl}^2 (the integral of f_{00}^2 as it appears in the denominator in (2.43)) and sum

over m and n . It is clear that the left hand sides become equal to $S^{+/-}$; this allows us to give exact expressions for the total membrane displacements.

$$S^+ = \frac{p_L + p_0}{\Lambda + \Gamma_+} \quad S^- = \frac{p_L - p_0}{\Lambda + \Gamma_-} \quad (2.56)$$

where we've defined the following quantities,

$$\Gamma_+ = \frac{\rho\omega^2}{k} \cot \frac{kL}{2}, \quad \Gamma_- = \frac{\rho\omega^2}{k} \tan \frac{kL}{2}, \quad \frac{1}{\Lambda} = \frac{1}{\pi a_{cyl}^2} \sum_{m=0}^{\infty} \sum_{n=1}^{\infty} \frac{(\int dS u_{mn})^2}{\Omega_{mn} \int dS u_{mn}^2}$$

We can finally write the membrane displacement as a function of the pressure inputs in the form

$$u_0(r, \phi; t) = G_{ipsi}(r, \phi)p_0 + G_{contra}(r, \phi)p_L \quad (2.57)$$

$$u_L(r, \phi; t) = G_{contra}(r, \phi)p_0 + G_{ipsi}(r, \phi)p_L \quad (2.58)$$

with the ipsilateral filter,

$$G_{ipsi} = \left(\frac{1}{\Lambda + \Gamma_+} + \frac{1}{\Lambda + \Gamma_-} \right) \sum_{n=1}^{\infty} \frac{\Lambda K_{mn}}{2} u_{mn}(r, \phi; t) \quad (2.59)$$

and the contralateral filter,

$$G_{contra} = \left(\frac{1}{\Lambda + \Gamma_+} - \frac{1}{\Lambda + \Gamma_-} \right) \sum_{n=1}^{\infty} \frac{\Lambda K_{mn}}{2} u_{mn}(r, \phi; t) \quad (2.60)$$

The total membrane displacement can also be expressed as a function of p_0 and p_L simply by integrating both sides of (2.57) and (2.58) giving us a new set of ipsi- and contralateral filters

$$G_{ipsi}^s = \left(\frac{1}{\Lambda + \Gamma_+} + \frac{1}{\Lambda + \Gamma_-} \right) / 2 \quad (2.61)$$

$$G_{contra}^s = \left(\frac{1}{\Lambda + \Gamma_+} - \frac{1}{\Lambda + \Gamma_-} \right) / 2 \quad (2.62)$$

The ipsilateral filter effectively gives us the response of the ipsilateral membrane when the contralateral membrane is blocked. Similarly, the contralateral filter gives us its response when there is no ipsilateral stimulus. These filters will play an important role in the evaluation of the model in the next chapter.

2.2.4 Circuit Model

Before we conclude this chapter, we will discuss the previous methods used to model ears coupled through an air cavity. This method was used by Christensen-Dalsgaard and

Manley in [4] and [5] and was based on methods presented in [16]. The method treats the problem through the analogy of electrical circuits and deals with low-frequency and high-frequency regimes separately.

In these models, the sound inputs are treated as voltage sources and the system is broken down into components, e.g. membranes, cavities, apertures which are modelled as lumped elements. Their impedance values depend on the geometry and material properties and in general can be resistive and reactive. The “current” is given by something called the “acoustic flow” which has the dimensions of volume per unit time. In the previous analysis, this is given by $j\omega\pi a_{cyl}^2 S^{0/L}$.

The low frequency circuit analog for the ICE model is illustrated in Fig. 2.9. The impedances are calculated using the following formulae,

$$R_T = \frac{\omega_T L_T}{Q}, \quad L_T = \frac{\rho_M d}{\pi a_{tym}^2}, \quad C_T = \frac{1}{\omega_T^2 L_T} \quad (2.63)$$

$$R_V = 0, \quad L_V = 0, \quad C_V = \frac{V_0}{\rho c^2} \quad (2.64)$$

where R , L and C are the resistance, impedance and capacitance of the quantities respectively with the total impedance given by $Z = R + j\omega L + 1/j\omega C$. ω_T is the first eigenfrequency of the membrane. It should immediately be apparent that the cavity impedance

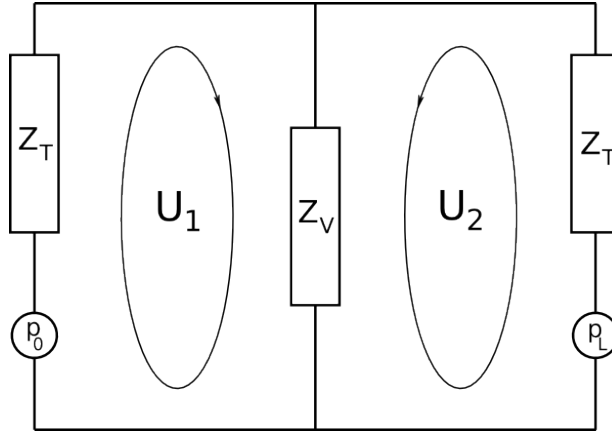


Figure 2.9: Low frequency circuit analog for the ICE-Model. The membrane impedances are denoted by Z_T and the impedance of the internal cavity is denoted by Z_V . The acoustic flows are given by U_1 and U_2 .

only depends on its volume. This is a result of the assumption that the air inside the cavity behaves like an adiabatic gas. The adiabatic equation of state can then be used to determine the instantaneous pressure from the instantaneous volume change due to the membrane motion which, after linearization, results in a uniform pressure inside the cavity. In addition, the membrane impedance Z_T only includes the effect of the first eigenmode. Also, Z_T includes the effect of the transducer which, in our case, is the extracolumella.

Upon solving the circuit equations, the acoustic flows are calculated to be,

$$U_1 = \frac{p_0(Z_T + Z_V) - p_L Z_V}{Z_T(Z_T + 2Z_V)}, \quad U_2 = \frac{p_L(Z_T + Z_V) - p_0 Z_V}{Z_T(Z_T + 2Z_V)}. \quad (2.65)$$

At first glance the above results look very similar to total membrane displacements shown in (2.57) and (2.58). In fact, we can find the equivalent impedances from our analysis by comparing U_0 and U_L with the above results,

$$Z_T^{eq} = \frac{1}{j\omega\pi a_{cyl}^2}(\Lambda + \Gamma_-), \quad Z_V^{eq} = \frac{1}{2j\omega\pi a_{cyl}^2}(\Gamma_+ - \Gamma_-) \quad (2.66)$$

We immediately see that in the equivalent membrane impedance there is a correction, Γ^+ which is a contribution of the cavity whereas in the circuit model, the membrane impedance is determined independent of the cavity. Moreover, the equivalent standalone membrane impedance, Λ , includes the influence of the higher modes. The equivalent cavity impedance becomes equal to Z_V at zero frequency and goes to infinity at the resonance frequencies of the cylinder, i.e at $\omega = n\pi c/L$, $n = 0, 1, 2 \dots$

We conclude this chapter by briefly stating the advantages of our method in comparison to the lumped element method -

- In terms of the membrane motion - we are able to account for the effect of asymmetrically loaded extracolumella and are able to describe the membrane motion in spatial detail.
- At low frequencies our model is consistent with the uniform pressure assumption but the nonuniformity steadily increases with frequency. We therefore have a single model that can describe both high- and low-frequency behaviour instead of treating the two regimes separately.

Chapter 3

Evaluation of the ICE–Model

We now have a complete geometrical representation of the ICE model as well as the analytical expressions u_0 and u_L that describe the membrane displacements in spatial detail as a function of direction and frequency. In this chapter we will use these variables to further study the features of our model and compare them with experimental results.

We start in Sec 3.1 by comparing the experimentally determined vibration pattern of the Tokay gecko’s eardrum with that of our model’s eardrum. In Sec. 3.2 we will briefly discuss the pressure distribution profile and eigenfrequencies of our cavity. In Sec 3.3 we will define and study the two main quantities that serve as important localization cues - the Internal Time Difference (iTD) and the Internal Level Difference (iLD). These values model the neural subtraction taking place in the animal’s brain which is the final step in localization. This is in contrast to the Interaural Time and Level Differences (ITD and ILD) that are entirely determined by the inputs to the two ears.

Parameter Estimation

Before we begin our analysis, we need to give numerical values to the parameters we first defined in 2.1. To do this we will simultaneously need to use experimentally determined values and estimate physical quantities that haven’t been measured based on experimental results. In our study we are primarily concerned with hearing in geckos. We will be using parameters (interaural separation, tympanum area etc.) from *Hemidactylus frenatus*, the common house gecko [5] and the Tokay gecko [4], [6]. The paramters are listed for both these species in Table 3.1.

Table 3.1: Geometry Parameters for the common house gecko (*Hemidactylus frenatus*) estimated from [5] and the Tokay gecko obtained from [4] and [6].

Parameter name	Hemidactylus	Tokay gecko
Length of the cylinder or interaural distance, L	10mm	22mm
Radius of the tympanic membrane, a_{tym}	1.2mm	2.2mm
Fundamental frequency (first eigenfrequency) of the tympanic membrane, ω_0	2800Hz	1700Hz
Quality factor of the tympanum, Q	1.2	1.2
Density of the membrane material, ρ_m	1mg/mm ³	1mg/mm ³
Thickness of the membrane, d	8μm	10μm
Volume of the cavity, V_0	.32ml	3.5ml
Extracolumella angle, β	$\pi/25$	$\pi/25$

As we can see, the house gecko, with an interaural separation of 10mm and mouth cavity volume of .32ml is a rather small lizard. The Tokay gecko is the second largest gecko species (interaural separation of 25.6mm and mouth cavity volume 3.5ml, [6]). Thus we will demonstrate the applicability of our model to animals hearing with widely varying head widths and mouth cavities. The geometric parameters, especially the head width and the membrane eigenfrequencies put important limits on the “hearing range” of our model as we will see in Sec. 3.3.

3.1 Spatial Vibration Pattern of the Membrane

We begin our analysis by evaluating the variation of the spatial vibration pattern of the tympanic membrane with frequency. The tympanic vibration pattern was first measured experimentally by Manley [17] for a *Tokay gecko* and was found to have the strongest response at around 1kHz. The measured vibration patterns are shown on the left in Fig. 3.1. Manley measured the vibration amplitude for eight locations on the membrane and measured the pattern seen on the left of Fig. 3.1. As we can see, at around 4kHz, the vibration pattern distinctly develops two maxima - something that would not happen to a centrally loaded tympanum except at frequencies well beyond the hearing range of geckos.

In order to compare our model with the experimental results, we plot the response of the ipsilateral membrane in our cylindrical ICE model calculated using (2.57). The input was chosen to be purely ipsilateral, meaning $p_L = 0$. This is illustrated in Fig. 3.1 (right) for the same frequency range as in the experimental data. The ipsilateral input was chosen to have unit amplitude and the model parameters used are given on the right most column of Table 3.1. The omitted region corresponds to the extracolumella.

The asymmetric nature of our membrane vibration pattern is a result of our chosen geometry. Mathematically this is a result of the fact that a uniform pressure (on the membrane surface) on a full circular membrane only couples to the circularly symmetric

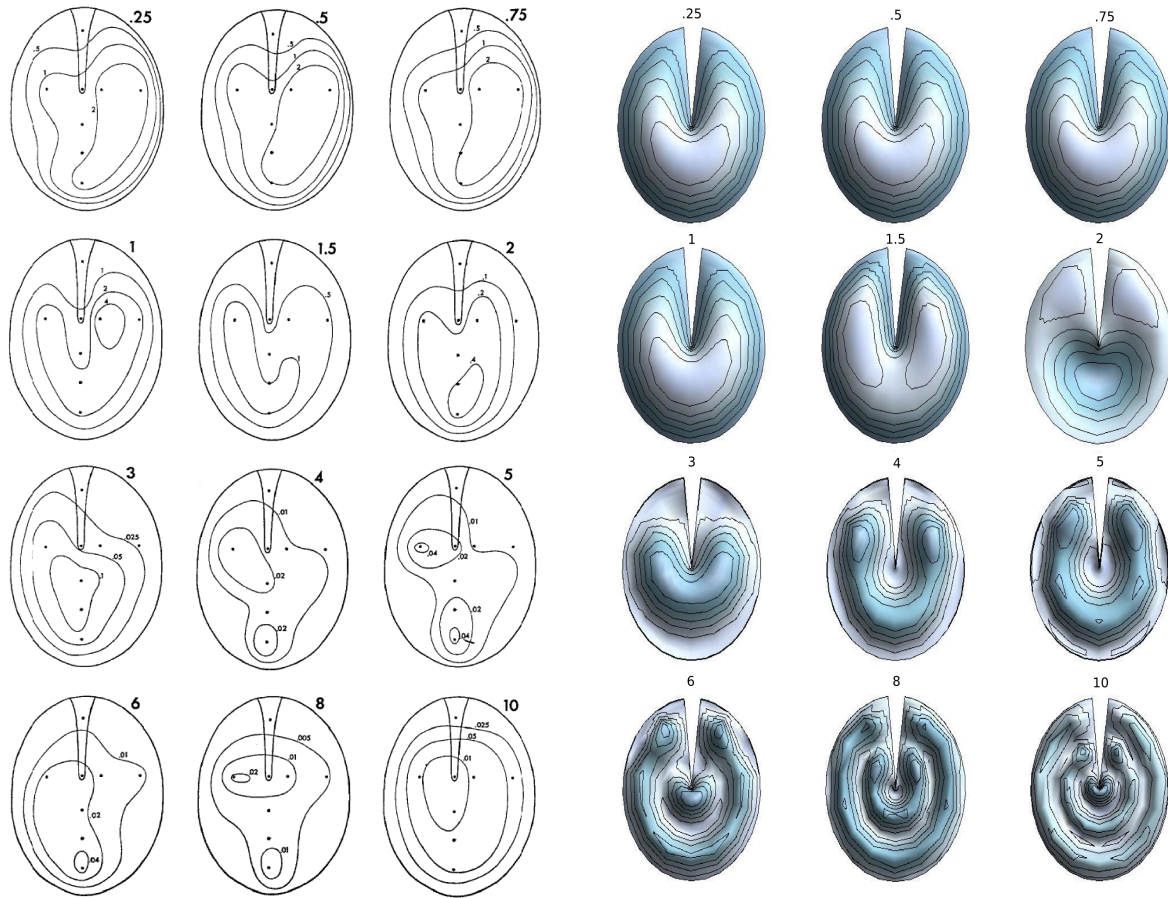


Figure 3.1: Experimental membrane vibration patterns of the Tokay gecko dependent on sound frequency varying from .5kHz to 10kHz. Data taken from [17].

J_0 modes. In the case of the sectoral membrane however, the uniform pressure couples to all the eigenmodes resulting in a more complex pattern. As a qualitative reproduction our model is very accurate but for a full quantitative analysis, we would need to account for the motion of the extracolumella. Moreover, the full mechanics of the extracolumella would also include its flection at higher frequencies.

3.2 Cavity Pressure Distribution

3.3 Directional Hearing Cues

3.3.1 Transmission Gain

3.3.2 Internal Time Difference

3.3.3 Internal Level Difference

Chapter 4

Conclusion

Bibliography

- [1] C. Voßen, *Auditory Information Processing in Systems with Internally Coupled Ears*. PhD thesis, Technische Universität München, 2010.
- [2] C. Voßen, J. Christensen-Dalsgaard, and J. L. van Hemmen, “Analytical model of internally coupled ears.,” *Journal of the Acoustical Society of America*, vol. 128, pp. 909–918, 2010.
- [3] G. Manley, “Frequency response of the middle ear of geckos,” *Journal of comparative physiology*, vol. 81, no. 3, pp. 251–258, 1972.
- [4] J. Christensen-Dalsgaard and G. A. Manley, “Directionality of the lizard ear,” *J. Exp. Biol.*, vol. 208, pp. 1209–1217, Mar 2005.
- [5] J. Christensen-Dalsgaard and G. Manley, “Acoustical coupling of lizard eardrums,” *Journal of the Association for Research in Otolaryngology*, vol. 9, no. 4, pp. 407–416, 2008.
- [6] J. Christensen-Dalsgaard, Y. Tang, and C. E. Carr, “Binaural processing by the gecko auditory periphery,” *J. Neurophysiol.*, vol. 105, pp. 1992–2004, May 2011.
- [7] C. Köppel and C. Carr, “Maps of interaural time difference in the chickens brainstem nucleus laminaris,” *Biological Cybernetics*, vol. 98, no. 6, pp. 541–559, 2008.
- [8] A. Michelsen and O. N. Larsen, “Pressure difference receiving ears,” *Bioinspiration & Biomimetics*, vol. 3, no. 1, p. 011001, 2008.
- [9] L. Rayleigh and A. Lodge, “On the acoustic shadow of a sphere. with an appendix, giving the values of legendre’s functions from p0 to p20 at intervals of 5 degrees,” *Philosophical Transactions of the Royal Society of London. Series A, Containing Papers of a Mathematical or Physical Character*, vol. 203, pp. pp. 87–110, 1904.
- [10] L. Rayleigh, *Theory of Sound: V. 1*. Dover Publications., 1900.
- [11] S. Rschevkin, O. Blunn, and P. Doak, *A Course OF Lectures On Sound*. Pergamon, 1963.
- [12] S. Temkin, *Elements of Acoustics*. Wiley, 1981.

- [13] E. T. Copson, *Introduction to the Theory of Functions of a Complex Variable*. Oxford: Clarendon Press, 1973.
- [14] C. Pozrikidis, *Fluid Dynamics: Theory, Computation, and Numerical Simulation*. Springer, 2009.
- [15] N. Asmar, *Partial Differential Equations with Fourier Series and Boundary Value Problems*. Pearson Education, Limited, 2005.
- [16] N. H. Fletcher, *Acoustic Systems in Biology*. Oxford: Oxford University Press, 1992.
- [17] G. A. Manley, “The middle ear of the tokay gecko,” *Journal of Comparative Physiology*, vol. 81, no. 3, pp. 239–250, 1972.

Acknowledgements

Danke.